# Joint Research Highlights

## Observation of the Orbital Quantum Dynamics in the Spin-1/2 Hexagonal Antiferromagnet $Ba_3CuSb_2O_9$

**M. Hagiwara and S. Nakatsuji**

In condensed matter physics, exploration of a novel quantum liquid state, such as Bose-Einstein condensation of cold atoms, superconductivity and quantum Hall state of electron systems, has been a subject of intense research both experimentally and theoretically. While many candidates of "quantum spin liquid" in which spin degrees of freedom does not freeze even at very low temperatures have been reported, almost no example has been found for an orbital liquid state, where the orbital degree of freedom remain fluctuating without lattice deformation down to a very low temperature. In our previous studies on the copper oxide 6H- $Ba_3CuSb_2O_9$ with a perovskite structure, we reported the first observation of striking absence of the static Jahn-Teller distortion down to the lowest temperature in this oxide based on copper (II), which is known as a strong Jahn-Teller active ion [1,2]. However, to date, the orbital dynamics have never been investigated.

In the present study, we have determined the frequency of the orbital quantum fluctuation in this compound by multi-frequency electron spin resonance (ESR) measurements in high magnetic fields [3]. We report the first determination of the orbital fluctuating frequencies, namely dynamic Jahn-Teller frequencies, at wide temperature range between 1.5 K and 100 K. The aforementioned results pave the way to investigate the dynamics of a new quantum liquid state named "quantum spin-orbital liquid" by multi-frequency ESR in high magnetic fields. The results demonstrate how high magnetic fields are useful for the studies on a quantum spin-orbital-liquid state.

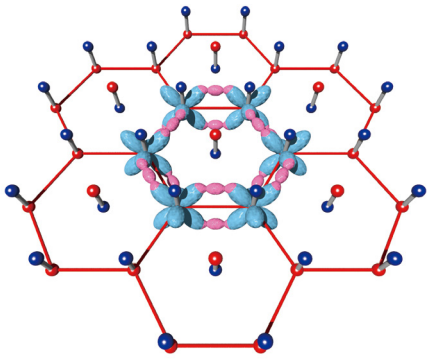

Fig. 1. The possible dynamic orbital states in the hexagonal sample, which form resonating singlet dimers in the honeycomb-based lattice. The light blue ovals show the temporally averaged special distribution of the copper orbitals.

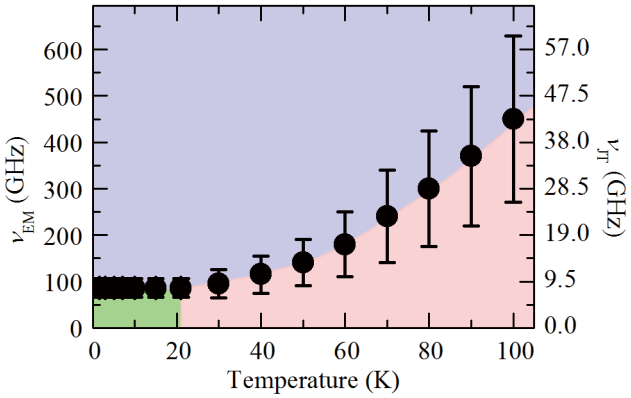


Fig. 2. Temperature dependence of the dynamic Jahn-Teller fluctuating frequency ($\nu_{JT}$) determined from the observed electromagnetic frequency ($\nu_{EM}$) where the ESR signal line shape changes from symmetric to asymmetric. The solid circles show the fluctuating frequencies at measurement temperatures, and the frequencies become constant (about 10 GHz, 100 picosecond) below 20 K, indicating the formation of the quantum liquid state.

**References**
[1] S. Nakatsuji *et al.*, Science **336**, 559 (2012).
[2] N. Katayama *et al.*, Proc. Natl. Acad. Sci. USA, **112**, 9305 (2015).
[3] Y. Han *et al.*, Phys. Rev. B 92, 180410R (2015).

**Authors**
M. Hagiwara[a] and S. Nakatsuji
[a]Osaka University

## Copper Oxide with No Static Jahn-Teller Distortion

**N. Katayama, H. Sawa, and S. Nakatsuji**

The quantum spin liquid (QSL) state has been intensively pursued since Anderson proposed the resonating valence bond model. For realizing a novel QSL state, orbital degree of freedom has been considered as a nuisance because orbital ordering usually appears at high temperature accompanying with a cooperative Jahn-Teller (JT) distortion and spin ordering. Therefore, the QSL candidates found so far have been mostly in spin only systems without orbital degree of freedom.

Perovskite-type 6*H*-$Ba_3CuSb_2O_9$ is a novel candidate material for the spin-orbital liquid state, which we have reported recently [1]. In the material, spin-orbital short-range ordering occurs in the short-range honeycomb lattice of $Cu^{2+}$ with $e_g$ orbital degrees of freedom, as shown in Fig.1(a). Powder x-ray diffraction experiment shows that even at low temperatures, the hexagonal components remain along with some orthorhombically distorted components. In the hexagonal phase, three-fold symmetry exists for the $Cu^{2+}$ sites which are surrounded by octahedrally coordinated oxygen, indicating the absence of a cooperative JT distortion.

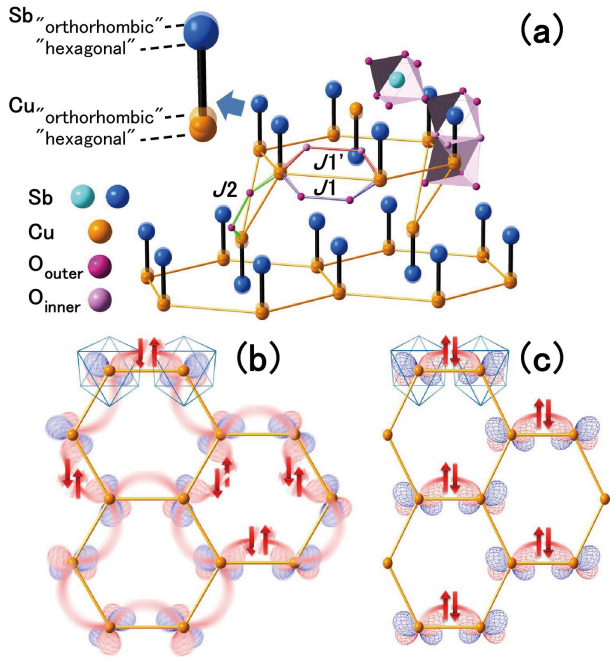


Fig. 1. (a) Schematic view of the local structure for hexagonal and orthorhombic samples. (b) Schematic picture of a *non*-cooperative static JT distortion. (c) and (d) Schematic pictures of spin-singlet formation in short-range honeycomb lattices of $Cu^{2+}$ for (c) hexagonal and (d) orthorhombic samples.

To explain this unusual feature, we proposed two possible scenarios. (i) Orbital glass state with a *non*-cooperative static JT distortion. In this scenario, the local symmetry is lowered by a static JT distortion, as schematically shown in Fig.1(b), but the overall hexagonal symmetry remains. (ii) Spin-orbital liquid state. The static JT distortion is absent and instead, a dynamic JT distortion appears, leading to a novel spin-orbital liquid state, as depicted in Fig. 1(c). These two possible scenarios cannot be distinguished by experimental results using powder specimens alone. A thorough structural study using a single crystal without orthorhombic components is required.

Our progress in preparing single crystalline samples enabled us to obtain single crystalline samples without any orthorhombic components down to the lowest temperature. Figures 2(a) and 2(b) show single crystal x-ray diffraction

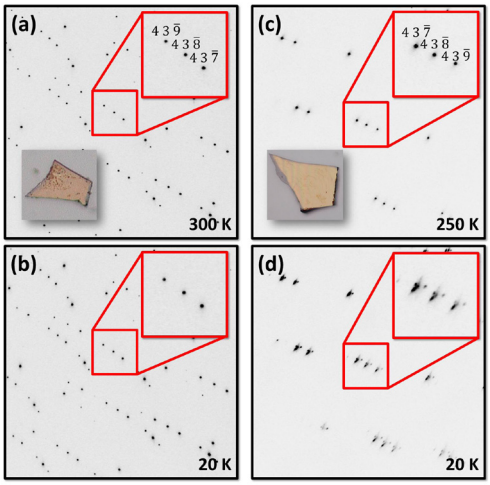


Fig. 2. Single crystal x-ray diffraction profiles for (a-b) hexagonal and (c-d) orthorhombic samples. The insets in (a) and (c) are photographs of the transparent brown single crystals for the hexagonal and orthorhombic samples, respectively. The hexagonal samples are darker than the orthorhombic samples.

experimental data. The peaks show no signs of splitting or broadening down to 20 K, the lowest temperature of our measurements ("hexagonal sample"). The hexagonal sample can be well refined by using the centro-symmetric space group $P6_3/mmc$ for all temperatures. For $P6_3/mmc$, the three-fold symmetry is retained for $Cu^{2+}$ sites, indicating the absence of the cooperative JT distortion. These observations are in sharp contrast with our previous single crystal x-ray diffraction study of 6*H*-$Ba_3CuSb_2O_9$. There, we reported that the Bragg peak splits into several separate reflections upon decreasing temperature, as shown in Figs. 2(c) and 2(d). This result indicates that the hexagonal $P6_3/mmc$ symmetry is lowered to the orthorhombic *Cmcm* symmetry ("orthorhombic sample"). We attribute this effect to a cooperative JT distortion induced by uniform ferro-orbital ordering of $Cu^{2+}$ ions (Fig.1(d)).

While x-ray diffraction experiment gives us the averaged structural information, the electron spin resonance (ESR) enables us to study the local orbital configuration. Using the single crystals, we confirmed the isotropic *g* factors are realized within the in-plane directions in the hexagonal samples down to 3.5 K, clearly indicating that the *non*-cooperative JT scenario is not realized and instead, a dynamic JT distortion appears [2]. Further studies using the crystals will address the open questions on the quantum spin-orbital liquid state, such as the orbital dynamics and the mechanism to stabilize such an exotic liquid state.

**References**
[1] S. Nakatsuji *et al.*, Science **336**, 559 (2012).
[2] N. Katayama *et al.*, Proc. Natl. Acad. Sci. USA, **112**, 9305 (2015).

**Authors**
N. Katayama[a], H. Sawa[a] and S. Nakatsuji
[a]Nagoya University

## Shot Noise Measurement of Local Fermi Liquid Out of Equilibrium

**R. Sakano, M. Ferrier, and K. Kobayashi**

Nine years after Millikan's monumental work on first observation of the elementary charge of the electron *e* in the famous oil drop experiment in 1909, Schottky also proposed an idea of measuring electric charge from the electron flow generated between two electrodes in a vacuum tube, by using statistical properties of electron counting and its fluctuation. For electric current generated by rare events (Poissonian process), the average current (*I*) is proportional to its fluctuations, namely, the shot noise (*S*), through the relation $S = 2e^*I$ where $e^*$ is the effective charge of the current carrying state.

Particularly, in condensed matter physics, many-body effect in conductor can generate nontrivial effective charges of their quasiparticle state, which has been studied in nano-sized electronic devices. For instance, fractional charges of Laughlin's quasiparticle in fractional quantum Hall systems, and double charge of cooper-pair in normal metal-superconductor junction were already detected in noise experiments.

By means of ultrasensitive current-noise measurement techniques, we recently succeeded in observing the shot noise and formation of effective charge states due to the spin Kondo effect in a carbon-nanotube quantum-dot, which is another typical many-body effect [1]. Applying small bias voltages between two electrodes connected to the quantum

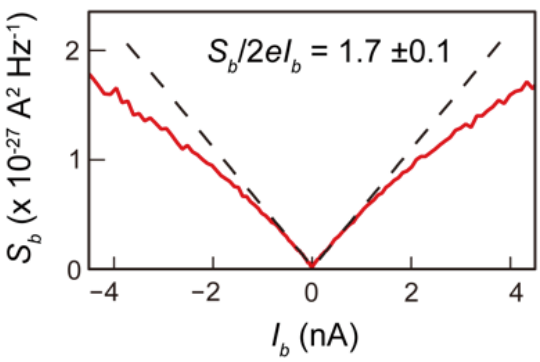


Fig. 1. The red solid line is the measured shot noise $S_b$ as a function of the backscattering current $I_b$ at 16 mK. The black broken line is $S_b = 2(1.7)eI_b$ .

dot containing a single electron, enhancement of current noise due to emergence of the Kondo effect in the quantum dot at low temperatures, is observed.

The averaged current and current noise in the Kondo dot can be described by the local Fermi liquid which is an extension of the Landau's Fermi liquid to impurities or quantum dots and the ground state of the Kondo effect. Tuning the dot level and the lead-dot mixings to hold the particle-hole symmetry, the bias-voltage linear response current shows perfect transmitting current due to the formation of quasiparticle's resonant level at the Fermi level, and this current does not fluctuate since no scattering occurs. Then, the leading nonlinear current is third order in bias voltages due to very small backscattering current ($I_b$). Thus, the current fluctuation from this nonlinear current ($S_b$) is found to follow the statistics of the Poissonian process. Theoretically, the noise emerges from three type of scattering processes described by the local Fermi liquid. First is the free quasiparticle's backscattering by the linewidth of the resonant level, with effective charge $e$. Second and third are backscattering of single quasiparticle and quasiparticle's pair by the residual interaction with effective charge $e$ and '$2e$,' respectively. In particular, the quasiparticle's pair scattering enhances the shot noise and effective charge of the non-equilibrium current through the Kondo quantum dot. The difference from fractional Hall states or superconducting states is that the Fermi liquid state has no energy gap at low energies. Thus mixture of the three scattering states with different effective charges composes the non-equilibrium current through the Kondo dot. As a consequence of two different effective charges in current, it is theoretically predicted that the noise-average ratio for the backscattering current takes the value $\frac{S_b}{2eI_b} = \frac{5}{3}$ in the Kondo limit [2-4].

The figure shows the observed shot noise as a function of the averaged backscattering current at 16 mK. For small currents noise-current ratio takes the values of $\frac{S_b}{2eI_b} = 1.70 \pm 0.1$, which is in very good agreement with the theoretical prediction. As mentioned above, this result corresponds to direct detection of quasiparticle pair creation in excited states of the local Fermi liquid. Furthermore, we investigate bias-voltage linear noises in the dot with particle-hole asymmetry and Fermi liquid parameters appearing in the averaged current, to ensure the accuracy of our shot noise measurement.

To conclude, our work offers a new approach to analyze excited states of electron correlated states though shot noise measurement in out of equilibrium systems.


**References**

[1] M. Ferrier T. Arakawa, T. Hata, R. Fujiwara, R. Delagrange, R. Weil, R. Deblock, A. Oguri, and K. Kobayashi, Nat. Phys. **12**, 230 (2016).
[2] E. Sela Y. Oreg, F. von Oppen, and J. Koch, Phys. Rev. Lett. **97**, 086601 (2006).
[3] A. O. Gogolin and A. Komnik, Phys. Rev. Lett. **97**, 016602 (2006).
[4] R. Sakano, T. Fujii, and A. Oguri, Phys. Rev. B **83**, 075440 (2011).



**Authors**

R. Sakano, M. Ferrier[a,b], T. Arakawa[a], T. Hata[a], A. Oguri[c], and K. Kobayashi[a]
[a]Osaka university
[b]University of Paris-Sud
[c]Osaka city university


## Electron-Beam-Patterned Lateral Schottky Gates on Atomically Thin $MoS_2$


**Y. Katagiri, T. Nakamura, and J. Haruyama**


$MoS_2$ is now attracting researchers' attention among so-called "two-dimensional materials" because it has a direct bandgap of 1.5-1.8 eV in the semiconducting phase (2H, trigonal prismatic $D_{3h}$). In the device application, the metallic phase (1T, octahedral $O_h$) part is indispensable for ohmic junctions or capacitor electrodes. The transition between the two phases does not have very high potential barrier and comparatively easily driven. Transition from 2H-phase to 1T phase caused by electron-beam (EB) irradiation has been recently observed [1].

For practical device installation, a lateral Schottky barrier (SB) forming at 2H-1T interface is desirable. Hence, the EB irradiated top-down fabrication of in-plane SB field effect transistors (SB-FETs) would be promising for $MoS_2$ based optical-electrical integrated circuits. Here we report forma-

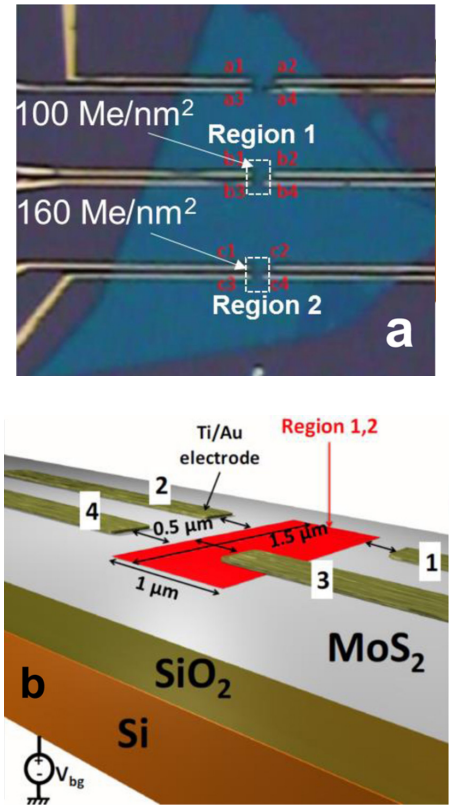


Fig. 1. (a) Optical microscope image of few-layer $MoS_2$, mechanically exfoliated from bulk, with two EB irradiation regions and two electrode pairs patterned on individual regions. (b) Schematic view of an electrode pair on one EB-irradiated region of (a).

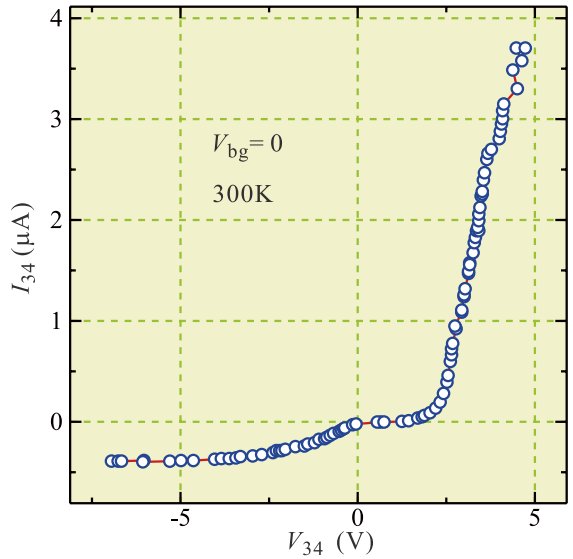


Fig. 2. Current-voltage characteristics between electrodes 3 and 4 in Fig. 1(b). The EB dose is 100 Me/nm$^2$.

tion of such a lateral SB junction with EB irradiation. From the current-voltage (I-V) characteristics, we believe the SB is formed at the designed position, which opens the way to 2D material integrated circuits.

Figure 1 (a) shows an optical micrograph of the sample. The $MoS_2$ layer can be observed as a blue triangular shape. Yellow lines are Ti/Au electrodes fabricated by EB-lithography. The rectangular regions indicated by the white-broken lines are for EB irradiation, the doses of which are also indicated. The detailed electrode configuration is illustrated in Fig.1 (b). Electrodes 1 and 2 are separated from the region of irradiation while electrode 3 is attached. Hence the SB diode characteristics should appear in the transport between electrodes 3 and 4. Figure 2 shows the I-V characteristics between electrodes 3-4. Clear single SB diode characteristics appears manifesting that the SB is formed between the irradiated region and electrode 4. Note that the SB between electrode 4 and $MoS_2$ has comparatively low resistance due to the large area and the high resistivity for the reverse bias region comes from the high quality lateral SB between the EB-irradiated 1T phase and 2H phase. The result indicates that we can make wirings and form SB-FETs at desired positions with this technique.

**References**
[1] Y. C. Lin *et al.*, Nature Nanotech. **9**, 391 (2014).
[2] Y. Katagiri *et al.*, Nano Lett. (2016) (doi: 10.1021/acs nanolett.6b01186).

**Authors**
Y. Katagiri[a], T. Nakamura, A. Ishii[a], C. Ohata[a], M. Hasegawa[a], S. Katsumoto, and J. Haruyama[a]
[a]Aoyama Gakuin University

# Scanning Tunneling Spectroscopy Study of Quasiparticle Interference on Dual Topological Insulator $Bi_{1-x}Sb_x$

**F. Komori, I. Matsuda, and Y. Ando**

Three-dimensional (3D) topological insulators (TIs) are characterized by a nontrivial topological invariant, which is protected by symmetry and the presence of a bulk band gap [1]. So far, two types of topological invariants have been found to be useful for finding 3D TIs. One is called $Z_2$ index and the other is mirror Chern number. A nontrivial $Z_2$ topology of the bulks state gives rise to spin-polarized metallic surface sates, which are protected by time-reversal symmetry. A nontrivial mirror Chern number defines a 3D topological crystalline insulator, which is associated with metallic surface states protected by mirror symmetry of the crystal and robust against TRS breaking. Insulators belonging to both of the topological phases may be called "dual" TIs. Bulk BiSb alloy is well known as a 3D $Z_2$ TI for x ~ 0.1-0.2, and this material has actually been predicted to be a dual TI. Although the electronic structure of the occupied surface states in BiSb has been well studied by means of angle-resolved photoemission spectroscopy (ARPES) [2], the structure of the whole surface bands including the unoccupied states has not been observed in pristine samples.

Measurements of the quasiparticle interference (QPI) using the Fourier-transform scanning tunneling spectroscopy (FT-STS), as shown in Fig. 1, is useful for elucidating the mirror Chern number of the BiSb alloy from the whole band structure [3]. The BiSb alloy would be suitable for the studies of both the spin texture and the change caused by surface magnetic impurities because the disorder in the electrostatic potential due to the alloying gives rise to QPI on the pristine surface. We clarified the dispersions of the unoccupied electronic states via the analysis of the QPI on the clean cleaved surface of BiSb as shown in Fig. 2. The absence of band crossing between $\Sigma_1$ and $\Sigma_2$ was elucidated, and the mirror Chern number is unambiguously determined to be -1. Co atoms deposited onto a clean surface lead to the

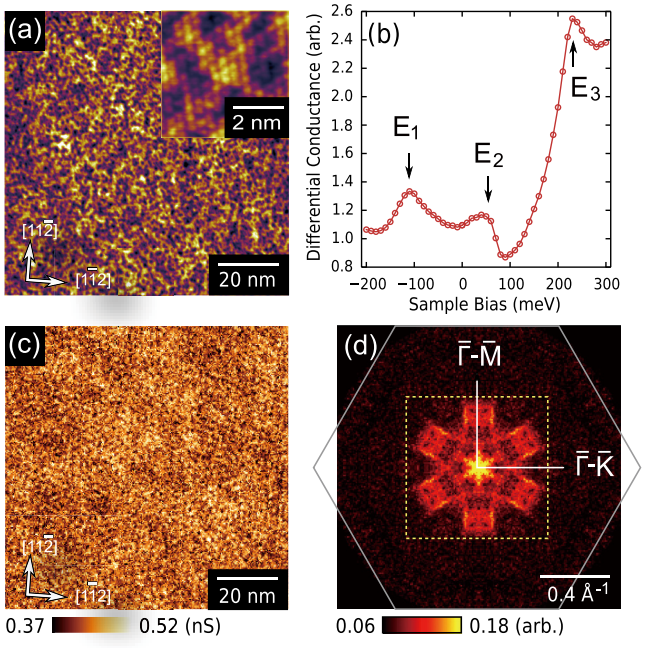


Fig. 1. (a) STM image of a region (93 x 93 nm$^2$) on a clean surface of $Bi_{1-x}Sb_x$ obtained at a constant current mode. (Setpoint: $I_t$ =200 pA at $V_b$ = 500 mV) The inset shows the close up image of a region (5 x 5 nm$^2$) revealing the hexagonal lattice of surface atoms. (Setpoint: 500 pA at 500 mV) (b) Average of 256 x 256 tunneling spectra measured on the same region. The peaks at E1, E2, and E3 are the van Hove singularities related to the surface bands. (Bias modulation: 7 mVrms at 396 Hz; Setpoint: 500 pA at 500 mV) (c) Spatial mapping of dI/dV at $V_b$ = +80 mV of the same region. (d) FT image calculated from the dI/dV in (c). All the equivalent points are averaged to increase signal-to-noise ratio. The hexagon represents the size and the orientation of the surface Brillouin zone. The dashed square represents the area displayed in the FT images in Fig. 2(a)-(d).

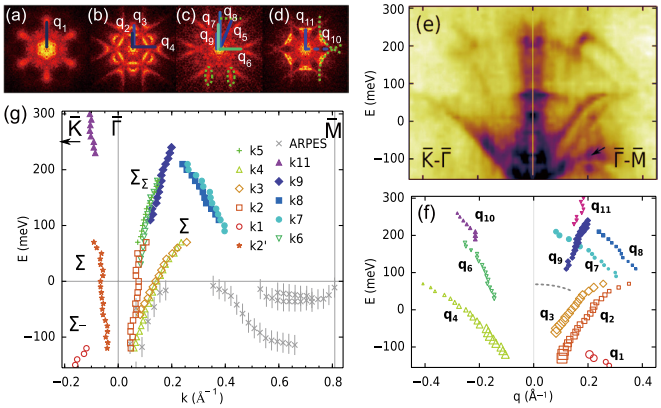


Fig. 2. (a)-(d) Fourie-transformation (FT) of dI/dV maps at E = -140 (a), -40 (b), +160 (c), and +260(d) meV on a clean surface of $Bi_{1-x}Sb_x$. The scattering vectors corresponding to the observed FT peaks are labeled by $q_1$-$q_{11}$. (e) Profiles of the FT images in the Γ-M and the Γ-K directions plotted in grayscale. The arrow at around -100 meV in the Γ-M direction indicate an artifact which disappears in the FT of (dI/dV )/(I/V ) maps. (f) Peak positions of the FT profiles. The size (area) of each marker is proportional to the peak intensity. Dashed line around 70 meV is a possible FT peak corresponding to QPI within the pocket along Γ-M, but not analyzed in detail. (g) Surface band structure of the clean surface of $Bi_{1-x}Sb_x$ reconstructed from our QPI data. Previous ARPES data [3] with an energy resolution of 18 meV are also plotted.

appearance of clover-leaf-like impurity states at around 80 meV above $E_F$. In spite of the deposition of the Co atoms on the surface, the results of QPI show no significant changes in the band dispersion from those for the clean surface. An enhancement of spin-conserving scatterings was detected through stronger QPI peaks in the FT spectrum.

**References**
[1] for review, Y. Ando, J. Phys. Soc. Jpn. **82**, 102001 (2013).
[2] F. Nakamura, *et. al.* , Phys. Rev. B **84**, 235308 (2011).
[3] S. Yoshizawa *et. al.*, Phys. Rev. B **91**, 045423 (2015).

**Authors**
F. Komori, S. Yoshizawa, F. Nakamura, A. A. Taskin[a], T. Iimori, K. Nakatsuji, I. Matsuda, and Y. Ando[a]
[a]Institute of Scientific and Industrial Research, Osaka University

# Oxygen Molecules Physisorbed on Ag(111) Surface: A two-dimensional Quantum Spin System

**Y. Kim, Y. Yoshida and, Y. Hasegawa**

An oxygen molecule ($O_2$) is one of the smallest molecular magnets with an S = 1 quantum spin, and thus an building block for attractive low-dimensional quantum spin systems, *i.e.*, quantum spin liquid phases and the Haldane phase. Recent development of scanning tunneling microscopy (STM) and spectroscopy (STS) has enabled direct access to the properties of single atoms and molecules and even their manipulation to fabricate artificial nanostructures, providing an ideal playground for bottom-up fabrication of the low-dimensional spin systems.

A well-known problem for $O_2$ adsorption on a substrate is that $O_2$ often loses its spin through the strong interactions with the substrate. However, it has been reported that the interaction between the physisorbed $O_2$ and Ag(111) surface is substantially weak and that structures almost identical to solid oxygen phases can be realized on the surface. Here we report the direct visualization of $O_2$ physisorbed on Ag(111) by using low-temperature STM/STS. Physisorption of the observed monolayer $O_2$ islands was confirmed by their thermal stability. We observed a well-ordered $O_2$ structure and found that the lattice was slightly distorted from an isosceles triangular shape, which can be explained by the presence of the exchange interactions between the $O_2$ spins. No Kondo resonance was observed in the differential tunneling conductance (d*I*/d*V*) spectra. Based on these observations, we conclude that the system is an S=1 two-dimensional antiferromagnetic quantum spin system

Figure 1 shows an STM image of $O_2$ on Ag(111) taken at 4.7 K. Because of the reduced local density of states monolayer $O_2$ island structures are observed as a depressed area. After the sample annealing up to 40 K, most of the $O_2$ islands disappeared, indicating physisorbed nature of the adsorbed molecules. The upper right panel of Fig. 1 shows a molecular-resolved image of the $O_2$ layer that exhibit a well-ordered lattice structure. One of the peculiar things we found is that the molecules form a scalene triangular lattice (i.e., AB < AC); the dimensions of the $O_2$ unit cell were measured as AB = 0.421 nm and AC = 0.435 nm based on real-space STM images taken on three different $O_2$ islands.

Since the $O_2$ lattice was incommensurate with the Ag(111) substrate, the surface corrugation of the substrate affects the $O_2$ lattice only as random perturbations, and thus does not seem to affect the shape of the $O_2$ lattice. Actually, an almost identical scalene triangular lattice was reported for low-coverage phase of $O_2$ physisorbed on HOPG, which is also incommensurate to the substrate. The similarity of the $O_2$ structures on two different substrates indicates that the distorted lattice structures are intrinsic to the $O_2$ molecules.

There should be some reason for the lattice distortion observed in the physisorbed $O_2$ layers. Here we considered exchange interactions between the $O_2$ spins. The energy of the exchange interactions between the $O_2$ spins was estimated as ~6 meV from the magnetization of solid oxygen. This was less than the van der Waals interactions (~30 meV) but significant enough to contribute to the total energy of the system. Indeed, the high-coverage phase of $O_2$/HOPG and solid oxygen showed lattice distortions coinciding with antiferromagnetic ordering, which indicates that the softness of the $O_2$ lattice allows the magnetic interaction to be involved in the lattice formation. With the magnetic ordering, the system can be stabilized by shortening the sides of the isosceles triangle at which spins are antiferromagnetically aligned, as schematically shown in Fig. 2. In order to confirm the scenario, we performed Monte Carlo simulations for the 2D freestanding $O_2$ lattice. Using

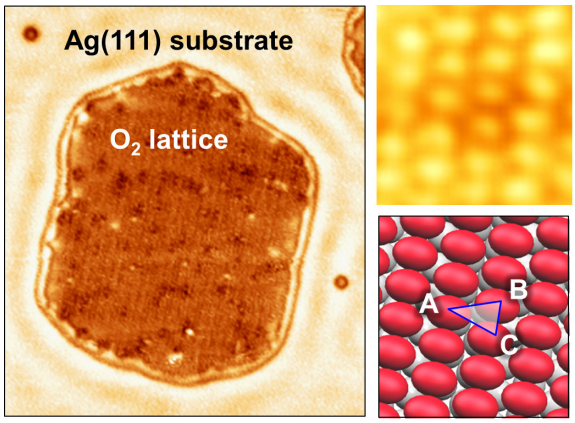


Fig. 1. (left) STM image acquired on $O_2$/Ag(111) at 4.7 K. An island structure is observed as a a depressed area. (upper right) Molecular resolved STM image in an $O_2$ island, (lower right) Schematic of $O_2$ lattice (red ellipsoids) on Ag(111).

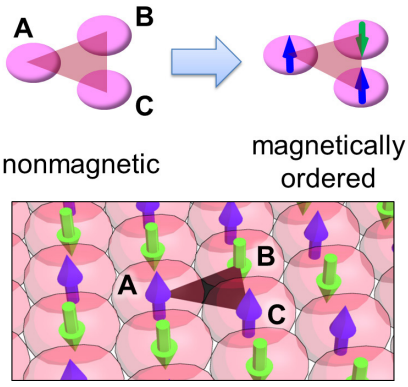


Fig. 2. Lattice distortion induced by antiferromagnetic ordering. The blue and green arrows denote the directions of the $O_2$ spins.

a set of the parameters that were used for the high-coverage phase of the $O_2$/HOPG, we successfully reproduced the distortion, confirming the validity of the scenario. We thus concluded that the antiferromagnetic ordering of the $O_2$ spins played a crucial role in the distortion of the $O_2$ lattice on Ag(111).

In order to verify the preservation of the intrinsic S=1 spin of $O_2$ on the Ag(111) surface, we also checked the d$I$/d$V$ spectra taken on the $O_2$ island and observed no specific evidence of the Kondo resonance around the Fermi level, in stark contrast with the case of $O_2$ molecules on Ag(110), which exhibits a clear Kondo resonance at 18 K. The $O_2$ spins are thus little influenced by the itinerant electrons of the substrate, and would be expected to form an S = 1 quantum spin system. These results imply that our system is an example of a 2D S = 1 antiferromagnetic quantum spin system and the potential for a brand-new approach of constructing low-dimensional quantum spin systems in a bottom-up fashion.

**References**

[1] S. Yamamoto, Y. Yoshida, H. Imada, Y. Kim, and Y. Hasegawa, Phys. Rev B **93**, 081408(R) (2016).

**Authors**

S. Yamamoto, Y. Yoshida, H. Imada[a], Y. Kim[a], and Y. Hasegawa

[a]RIKEN

# Novel Pressure Dependence of the Superconductivity in Non-Centrosymmetric $LaNiC_2$: Evidence of Strong Electronic Correlations

**S. Katano and Y. Uwatoko**

Since the discovery of the heavy-fermion superconductor $CePt_3Si$ [1], superconductivity of non-centrosymmetric systems has attracted great interest. The non-centrosymmetry causes the antisymmetric spin-orbit coupling (ASOC) that leads to the indistinguishability of spin-singlet and spin-triplet electron pairings. $LaNiC_2$ forms a non-centrosymmetric structure (space group: orthorhombic *Amm2*), and exhibits superconductivity below the transition temperature $T_c$ of about 3 K. On this superconductivity a recent muon spin relaxation (μSR) experiment indicated the breaking of the time-reversal symmetry (TRS) in the superconducting state, which leads to non-unitary *p*-wave spin-triplet pairings [2]. However, a NQR study suggested an enhancement of the nuclear spin relaxation rate ($1/T_1$) just below $T_c$, implying

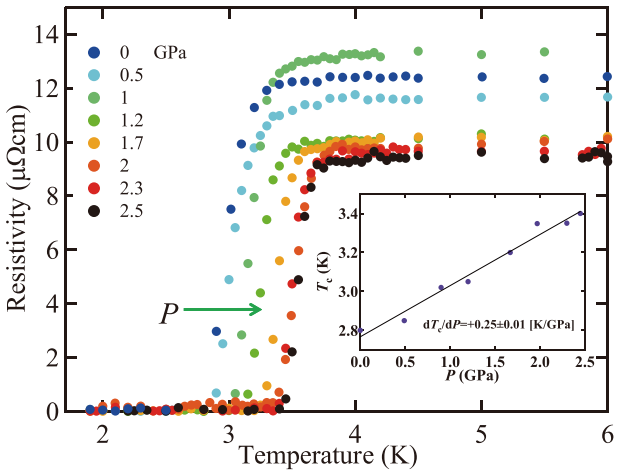


Fig. 1. Electrical resistivity under high pressures up to about 3 GPa. The inset shows that pressure enhances the superconducting transition temperature $T_c$ substantially.

a conventional BCS-type superconductor [3]. Therefore its superconducting mechanism is still unclear. Furthermore, this system is not magnetic, and thus it has been considered that its electronic correlations would be weak in contrast with other heavy fermion systems. To get further information on this superconductivity, pressure effects on the superconducting state of $LaNiC_2$ have been studied.

Figure 1 shows the temperature dependence of the electrical resistivity of $LaNiC_2$ under high pressures up to 3 GPa. Under these pressures, $T_c$ is enhanced greatly at the rate of 0.25 K/GPa. For normal conventional metals pressure contracts their lattices, and generally the electron density $D(E_F)$ at the Fermi energy $E_F$ decreases. In the BCS theory, therefore, $T_c$ would decrease with increasing pressure. The results obtained here thus suggest that the superconductivity of this system is possibly changed under high pressure by some novel mechanism.

Above the pressure of 3 GPa, the superconductivity enhanced once is heavily suppressed. As shown in Fig. 2, the pressure of 8 GPa extinguishes its superconductivity completely. At the higher temperatures, on the other hand, the resistivities above 5 GPa show clear anomalies over 100 K, as displayed in the inset of Fig. 2. The temperature observed as an anomalous hump increases with pressure up to room temperature at the rate of 51.5 K/GPa. These results show that a new state (NS) is evidently induced under high

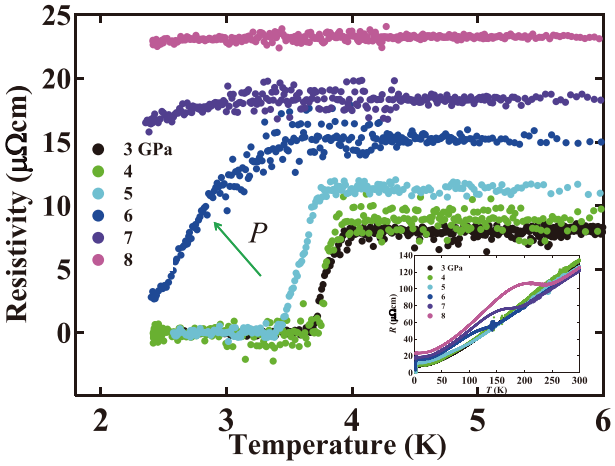


Fig. 2. Electrical resistivity under high pressures up to 8 GPa. The inset indicates that the resistivity at high temperatures shows an anomaly with a clear hump, implying an emergence of a new state.

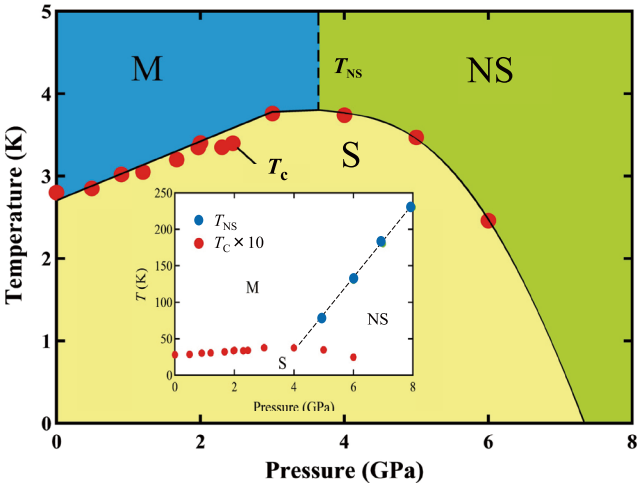


Fig. 3. *P-T* phase diagram of $LaNiC_2$. The mark M and S denote metal and superconductivity, respectively; and NS indicates 'a new state' induced under pressure. In the inset, the superconducting transition temperatures are multiplied by the factor of 10.

pressures. With such an emergence of the NS state, the superconductivity is intensely suppressed. Figure 3 shows the phase diagram obtained. It is noted that this diagram shows a dome for $T_c$ but is *mirror symmetric* to those of many other systems like heavy-fermion and high-*T*c superconductors.

For this NS state it remains that some $RNiC_2$ (*R* = rare-earth) systems show charge density wave (CDW) states at high temperatures. Thus, it might be natural that the anomalous hump observed at the temperatures over 100 K originates from the phase transition to the CDW state. This newly induced state is enhanced strongly under high pressures; further, that is quite robust up to the highest pressure of 30 GPa investigated in this work.

With the disappearance of the superconductivity a new state (NS) with a high energy scale is dramatically emerged. These results indicate that the system is not a simple normal metal but is highly correlated with strong electronic interactions such as CDW, which correlations may contribute to the superconductivity of this unique system [4].


**References**

[1] E. Bauer *et al.*, Phys. Rev. Lett. **92**, 027003 (2004).
[2] A.D. Hillier, J. Quintanilla, and R. Cywinski, Phys. Rev. Lett. **102**, 117007 (2009).
[3] Iwamoto *et al.*, Phys. Lett. A **250**, 439 (1998).
[4] S.Katano *et al.*, Phys. Rev. B **90**, 220508(R) (2014).



**Authors**

S. Katano[a], H. Nakagawa[a], K. Matsubayashi, Y. Uwatoko, H. Soeda[b], T. Tomita[b], and H. Takahashi[b]
[a]Saitama University
[b]Nihon University


## Correlation Effects in Topological Insulators


**N. Kawakami**



We report our recent studies on correlated topological insulators using ISSP supercomputer. We first investigate a topological Mott insulator in one dimension (1D) to discuss how the edge Mott states emerge due to the interplay of topology and correlation [1]. We then address how the topological state is restored by the temperature in the presence of strong correlations in two dimensions (2D)


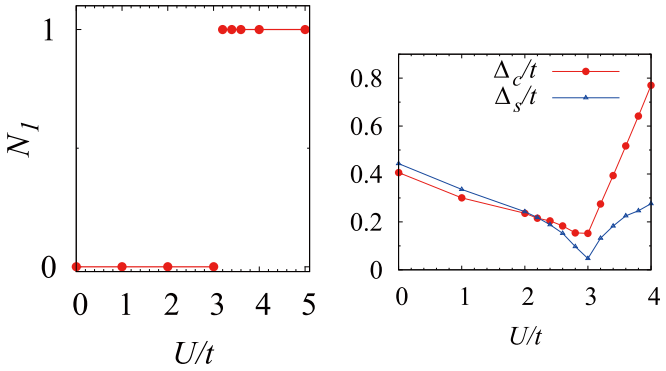


Fig. 1. Left panel: winding number $N_1$, Right panel: spectral gaps for edge states:$\Delta_c$, ($\Delta_s$) for the one-particle (spin excitation) spectrum [1], as a function of Hubbard interaction *U* (*t* denotes nearest neighbor hopping). It is seen that the topological phase transition occurs, but $\Delta_c$ does not vanish in contrast to a noninteracting topological transition. Instead, we see the gap closing for collective spin excitations $\Delta_s$.

[2]. We demonstrate that such restoration of topological properties is rather generic, by exploring another correlated topological insulator [3]. We also mention some issues related to topological insulators [4-6].

(A) We first summarize the results obtained for a 1D topological Mott insulator [1]. By examining the bulk topological invariant and the entanglement spectrum of a correlated Su-Schrieffer-Heeger model, we clarify how gapless edge states in a non-interacting topological band insulator evolve into spinon edge states in a topological Mott insulator. Furthermore, we propose a new type of topological Mott transition. In Fig.1, we show a topological Mott transition driven by the Hubbard interaction *U* [1]. As seen from left panel, a transition from a trivial phase ($N_1$=0) to a nontrivial one ($N_1$=1) occurs, and at this transition a one-particle gap ($\Delta_c$) is not closed but only a spin excitation gap ($\Delta_s$) becomes gapless (right panel). This unconventional transition occurs in a spin liquid phase and is accompanied by zeros of the single-particle Green's function and a gap closing in the spin excitation spectrum [1].

(B) We elucidate how a topologically nontrivial phase evolves at finite temperatures [2,3]. Specifically, we study a Kane-Mele Kondo lattice model at finite temperatures with dynamical mean field theory. The obtained phase diagram shows three phases at zero temperature [2]: an antiferromagnetic topological insulator, an antiferromagnetic trivial insulator, and a trivial Kondo insulator. We find a restoration of topological properties at finite temperatures due to the interplay of a topologically nontrivial structure and electron correlation. In order to address this phenomenon, we analyze the bulk and edge properties. In the bulk, the spin-Hall conductivity which is almost zero around zero temperature increases with increasing temperature. At the edge, the gapless edge modes emerge with increasing temperature.

(C) We finally summarize some issues related to topological phase transitions, which will be realized in new platforms such as cold atomic systems, photonic systems, etc. We clarify non-equilibrium topological phase transitions in 2D optical lattices [4]. We unveil hidden topological phases in a 1D quantum walk [5]. We clarify topological properties of cold bosons in 1D quasiperiodic optical lattices [6].


**References**

[1] T. Yoshida, R. Peters, S. Fujimoto, and N. Kawakami, Phys. Rev. Lett. **112**, 196404 (2014).
[2] T. Yoshida, R. Peters, and N. Kawakami, Phys. Rev. B **93**, 045138 (2016) .

[3] T. Yoshida and N. Kawakami, arXiv:1604.00122.
[4] M. Nakagawa and N. Kawakami, Phys. Rev. A **89**, 013627 (2014); Phys. Rev. Lett. **115**, 165303 (2015).
[5] H. Obuse, J. K. Asboth, Y. Nishimura, and N. Kawakami, Phys. Rev. B **92**, 045424 (2015).
[6] F. Matsuda, M. Tezuka, and N. Kawakami, J. Phys. Soc. Jpn. **83**, 083707 (2014) .

**Authors**
N. Kawakami[a], T. Yoshida[a], R. Peters[a], N. Nakagawa[a], F. Matsuda[a], M.Tezuka[a], Y. Nishimura[a], S. Fujimoto[b], H.Obuse[c], and J. K. Asboth[d]
[a]Kyoto University of Tokushima
[b]Osaka University
[c]Hokkaido University
[d]Wigner Research Center, Hungary

# Investigation of Average and Local Structures, and Electron-Density Distribution of Lithium Transition-Metal Oxide

**Y. Idemoto and N. Kitamura**

In recent years, the lithium-ion battery has been expected to be applied for not only portable electronic devices such as a mobile phone but also a vehicle and a storage device and so on. From such background, many researches have devoted their efforts to develop new lithium transition-metal oxides with superior cathode performances. For the development, crystal and electronic structures of the cathode materials must be determined precisely since the structures are well known to affect the cathode properties. Moreover, it is considered recently that local orderings of transition metals in the crystal play an important role for charge and discharge processes. Therefore, it is highly expected to discover local structures hidden in crystal structures. In our recent works, we paid special attention on $LiNi_{0.8}Co_{0.2}O_2$-based materials [1] and $Li(Li_{1/6}Mn_{1/2}Ni_{1/6}Co_{1/6})O_2$ [2] with the layered structure, and investigated the average and local atomistic structures, and electron-density distribution by using neutron and synchrotron X-ray sources.

As for $LiNi_{0.8}Co_{0.2}O_2$-based materials, we refined the average structure by the Rietveld analysis using neutron diffraction patterns. The data were measured under ambient condition with HERMES installed at JRR-3. Fig. 1 shows the Rietveld refinement pattern of $LiNi_{0.79}Zn_{0.01}Co_{0.2}O_2$. In the analysis, we assumed the space group as $R$-3$m$, and optimized an exchange amount of Li and Ni, which is the so-called "cation mixing". As a result, the average structure could be successfully refined, and the Ni content at Li site was estimated as 0.056 (3). We could also refined average structures of other $LiNi_{0.8}Co_{0.2}O_2$-based materials with partial Cu substitution and without any substitution (the pristine sample) in the same manner. For the purpose of electronic-structure analysis on the samples, we carried out the maximum-entropy method (MEM) using synchrotron X-ray diffraction patterns. When X-ray diffraction data are used, it is quite difficult to obtain accurate information on light element such as Li and O generally. Therefore, the average structures refined with the neutron diffractions were utilized as the initial structures in the analytical processes. By this strategy, electron-density distributions could be estimated successfully, and then it was found that both the Zn and Cu substitution for $LiNi_{0.8}Co_{0.2}O_2$ tended to reduce a bond strength between the transition-metal and oxygen sites.

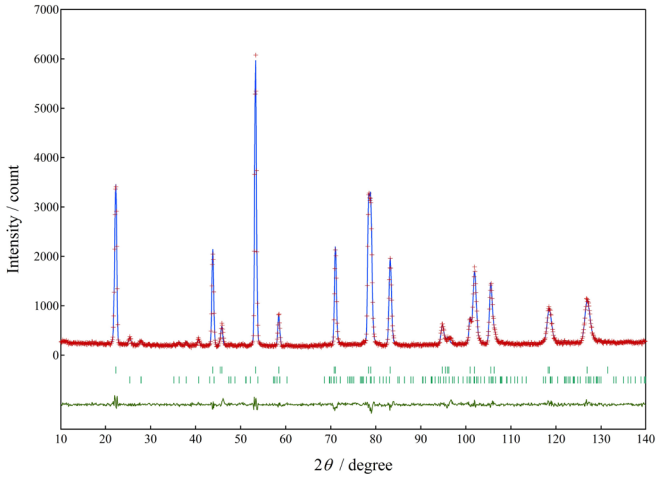


Fig. 1. Rietveld refinement pattern of $LiNi_{0.79}Zn_{0.01}Co_{0.2}O_2$. Red pluses and a blue solid line represent observed and calculated intensities, respectively. Vertical marks indicate positions of allowed Bragg reflections (upper marks for $LiNi_{0.79}Zn_{0.01}Co_{0.2}O_2$, and lower marks for $Li_2CO_3$). A curve at the bottom is a difference between the observed and calculated intensities in the same scale.

In order to investigate the local structure of $Li(Li_{1/6}Mn_{1/2}Ni_{1/6}Co_{1/6})O_2$ with the layered structure, we firstly performed the average structure refinement (S. G.: $C2/m$) using neutron Bragg profile recorded at HERMES, and then analyzed the reduced pair distribution function, $G(r)$, which was derived from neutron total scatterings. Prior to the PDF fitting, we constructed the some local-structure models with different metal arrangement which satisfied the site occupancies refined by the Rietveld method, and then relaxed atomic configurations of the models by the density functional theory (DFT) calculation. On the basis of the results, we carried out the PDF fitting only for an energetically-stable model. The PDF analysis indicated that a $LiMn_6$ ordering was formed within the transition-metal layer in the same way as $Li_2MnO_3$. In addition, the detailed investigation suggested a local distortion along the $c$ axis which is perpendicular to the layer.

The our works described above demonstrate that the structure analysis using both the neutron and synchrotron X-ray diffractions gives us fruitful information the electronic structure as well as the crystal structure of the cathode materials for the lithium-ion battery. Moreover, a combination of the Rietveld and PDF analyses enable us to gain deeper understanding the atomic configurations of the functional oxides.

**References**

[1] Y. Idemoto, Y. Tsukada, and N. Kitamura, Solid State Ionics, **279**, 6 (2015).
[2] Y. Idemoto, K. Akatsuka, and N. Kitamura, J. Power Sources, **299**, 280 (2015).

**Authors**
Y. Idemoto[a] and N. Kitamura[a]
[a]Tokyo University of Science

# Extremely Large and Anisotropic Upper Critical Field inIon-Gated $MoS_2$

**Y. Saito, Y. Kohama, and Y. Iwasa**

Superconductivity is a quantum phenomenon characterized by zero electrical resistance and complete expulsion of the magnetic flux. The extraordinary properties arise from the condensation of the Cooper pair that consists of a pair

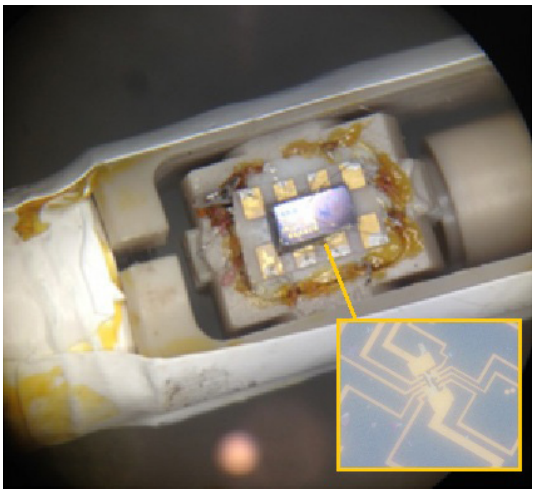

Fig. 1. $MoS_2$ EDLT transistor on the rotator probe.

of free electrons with opposite spins. The application of strong magnetic fields tends to arrange spins in one direction, therefore the ordinal superconductivity cannot be survived above the certain limit of magnetic fields, called the Pauli limit "$H_{Pauli}$ ~ 1.86 $T_c$". Nevertheless, our recent collaboration work performed at International MegaGauss Science Laboratory (IMGSL) has experimentally revealed that an ion-gated molybdenum disulphide ($MoS_2$) transistor exhibits an extremely large upper critical field ($H_{c2}$) that is 4-5 times more than the Pauli limit of ~ 12 T [1].

The $H_{c2}$ were directly estimated from the magnetoresistance measurement on superconducting $MoS_2$ samples that were prepared by using an electric-double-layer transistor (EDLT) configuration [2]. Since the $H_{c2}$ is extremely large and shows a high degree of anisotropy, we developed a specially designed plastic rotator (see Fig.1) and performed magnetoresistance measurements in pulsed magnetic fields up to 55 T. The rotator probe was made of a plastic material, and thus the eddy current related problems, such as Joule heating and mechanical vibration, were completely eliminated even in a pulsed field environment.

The obtained $H_{c2}$ vs $T$ plot is shown in Fig.2, which provides the experimental evidence of anisotropic and extremely large upper critical fields on the $MoS_2$-EDLT. We interpret that the large anisotropy can be understood as a consequence of the two-dimensional electric property of $MoS_2$-EDLT, namely the completely different orbital motion

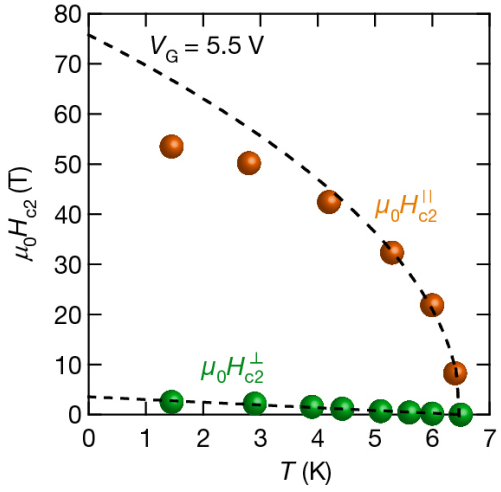


Fig. 2. Upper critical fields ($H_{c2}$) vs Temperature ($T$). The orange and green dots are the $H_{c2}$ when the external magnetic fields are applied to parallel ($H_{c2}^{\parallel}$) and perpendicular ($H_{c2}^{\perp}$) to the plane, respectively. The upper critical fields were deduced from the magnetoresistance measurements.

for the in-plane and out-of-plane configurations. On the other hand, the exceptionally large $H_{c2}$ for the in-plane configuration is due to an enhancement of the Pauli limit, caused by the strong spin-orbit interaction and the non-centrosymmetric nature of $MoS_2$ single layer. Indeed, our numerical calculation based on realistic tight-binding calculations demonstrate that the Cooper pairs are protected by the strong spin-orbit interaction, and are thereby very robust against external magnetic fields for the in-plane configuration. The robustness of $H_{c2}$ against external magnetic fields might make $MoS_2$-EDLT an ideal platform for investigating noncentrosymmetric superconductors.


**References**

[1] Y. Saito, Y. Nakamura, M. S. Bahramy, Y. Kohama, J. T. Ye, Y. Kasahara, Y. Nakagawa, M. Onga, M. Touanga, T. Nojima, Y. Yanase, and Y. Iwasa, Nature Physics **12**, 144 (2016).

[2] J. T. Ye, Y. J. Zhang, R. Akashi, M. S. Bahramy, R. Arita, and Y. Iwasa, Science **338**, 1193 (2012).



**Authors**

Y. Kohama, Y. Saito, Y. Iwasa, M. Tokunaga, and K. Kindo


## Quantum Transport of Dirac Fermions Coupled with Magnetic Order in $EuMnBi_2$


**H. Sakai, M. Tokunaga, and S. Ishiwata**


Dirac materials, characterised by linear energy-momentum dispersion near Fermi level, have attracted much attention for their unique transport properties such as half-integer quantum Hall effect, observable even at room temperature in graphene. To expand potential application of their distinct quantum transport, it is highly desirable to control the conduction of Dirac fermions by magnetic moments in solids as well as external fields. Despite recent discoveries of a number of new bulk Dirac materials, quantum transport features have been elucidated mostly in nonmagnetic materials, as exemplified by so-called Dirac/Weyl semimetals, such as $Cd_3As_2$, $Na_3Bi$, and TaAs.

We here report novel magneto-transport features for a

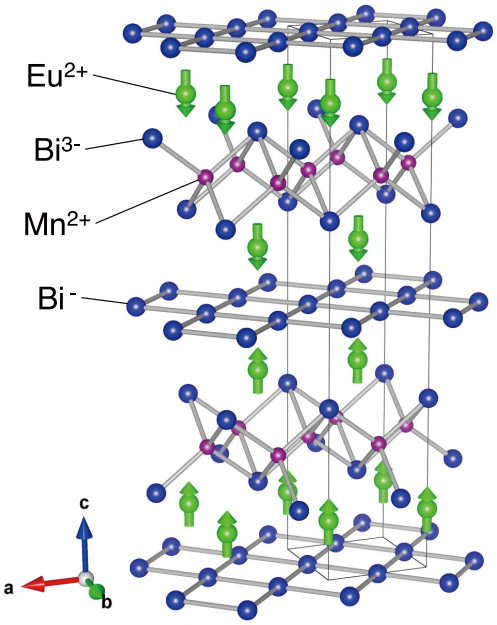


Fig. 1. Schematic illustration of the crystal and magnetic structure for $EuMnBi_2$ at zero field, together with the formal valence of each ion. The magnetic moments of the Mn sublattice are not shown for brevity.

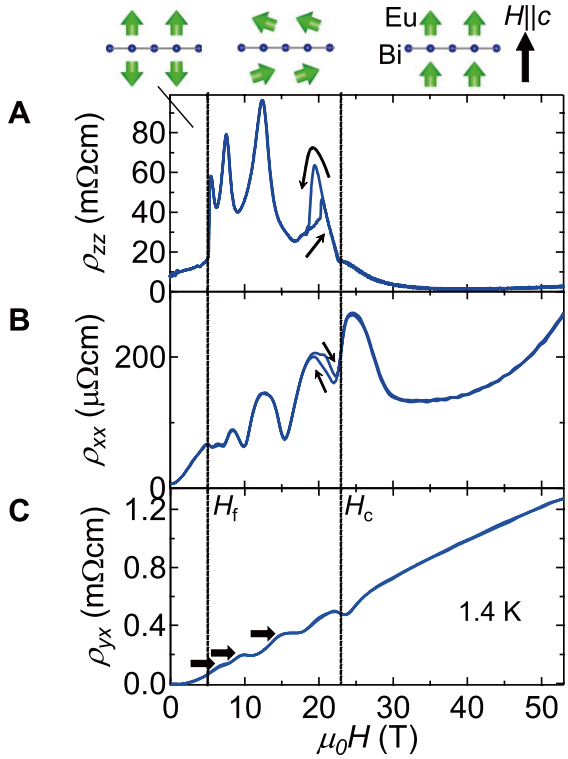


Fig. 2. Field profile of (A) interlayer resistivity $\rho_{zz}$, (B) in-plane resistivity $\rho_{xx}$, and (C) Hall resistivity $\rho_{yx}$ for $EuMnBi_2$ at 1.4 K for the field parallel to the *c* axis. Schematic illustration of variation of the ordered Eu moments adjacent to the Bi layer is presented above the panels.

new multilayer Dirac fermion system $EuMnBi_2$. Recently, layered magnets $AMnBi_2$ ($A$=$Sr^{2+}$ [1-3] and $Eu^{2+}$ [4,5]) were found to host anisotropic 2D Dirac fermion, providing an ideal arena to reveal the interplay between Dirac fermions and ordered magnetic moments. The crystal structure consists of the conducting layers of Bi square net hosting quasi two-dimensional (2D) Dirac fermions and the insulating magnetic layers consisting of the Mn-Bi and *A* layers (Fig. 1). To explore quantum transport phenomena associated with magnetically-controllable Dirac fermions, we have investigated the detailed magnetic and transport properties by applying field up to 55 T at the International MegaGauss Science Laboratory at the Institute for Solid State Physics [6].

The magnetization dominated by the Eu sublattice shows typical behaviour of uniaxial antiferromagnet. We observed a spin-flop transition for the field of ~ 5.5 T ($H_f$) along the *c* axis, followed by saturation at ~ 22 T ($H_c$) with a saturation moment of ~ 6.5 $\mu_B$/f.u (not shown here), which reflects the full moment of localised Eu 4*f* electrons. The in-plane resistivity ($\rho_{xx}$) and interlayer resistivity ($\rho_{zz}$) exhibit clear anomalies at the magnetic phase transition of Eu sublattice (Fig. 2). In particular, $\rho_{zz}$ exhibits a large jump at $H_f$, followed by giant Shubnikov–de Haas (SdH) oscillations that reach $\Delta\rho_{zz}/\rho_{zz}$ ~ 50% in the spin-flop antiferromagnetic (AFM) phase (Fig. 2A). This high $\rho_{zz}$ state is terminated at $H_c$, above which the $\rho_{zz}$ value is substantially reduced. Interestingly, the magnitude of the SdH oscillations in $\rho_{xx}$ and $\rho_{yx}$ (Hall resistivity) is also enhanced in the spin-flop AFM phase (Fig. 2B and 2C), which evolves to plateau-like structures in the $\rho_{yx}$ profile as indicated horizontal thick arrows in Fig. 2C. This signifies the first observation of the multilayer quantum Hall effect of quasi 2D Dirac fermions in a bulk magnet [6].

In spite of the strong coupling between the magnetism and transport properties, the carrier mobility is estimated to be as high as μ ~ 14,000 $cm^2$/Vs at 2 K. This indicates that the interlayer conduction is suppressed by the staggered Eu moments along the *c* axis, whereas the ferromagnetic order within the plane may promote the in-plane transport. Thus, the crystal structure of $EuMnBi_2$ can be regarded as a natural spin-valve structure embedded in a multilayer Dirac fermion system. Our discovery would open the door for engineering the Dirac fermion transport in magnetic materials suitable for novel spintronic devices with an extremely high speed.

**References**

[1] J. Park, G. Lee, F. Wolff-Fabris, Y. Y. Koh, M. J. Eom, Y. K. Kim, M. A. Farhan, Y. J. Jo, C. Kim, J. H. Shim, and J. S. Kim, Phys. Rev. Lett. **107**, 126402 (2011).
[2] J. K. Wang, L. L. Zhao, Q. Yin, G. Kotliar, M. S. Kim, M. C. Aronson, and E. Morosan, Phys. Rev. B **84**, 064428 (2011).
[3] K. Wang, D. Graf, H. Lei, S. W. Tozer, and C. Petrovic, Phys. Rev. B **84**, 220401(R) (2011).
[4] A. F. May, M. A. McGuire, and B. C. Sales., Phys. Rev. B **90**, 075109 (2014).
[5] S. Borisenko, D. Evtushinsky, Q. Gibson, A. Yaresko, T. Kim, M. N. Ali, B. Buechner, M. Hoesch, and R. J. Cava, arXiv: 15070.04847 (2015).
[6] H. Masuda, H. Sakai, M. Tokunaga, Y. Yamasaki, A. Miyake, J. Shiogai, S. Nakamura, S. Awaji, A. Tsukazaki, H. Nakao, Y. Murakami, T.-h. Arima, Y. Tokura, and S. Ishiwata, Sci. Adv. **2**, e1501117 (2016).

**Authors**
H. Masuda[a], H. Sakai[b,a], M. Tokunaga, A. Miyake, and S. Ishiwata[a,c]
[a]The University of Tokyo
[b]Osaka University
[c]Presto

## A New Numerical Method for Finite-Temperature Calculations of Strongly Correlated Electrons Systems

**T. Misawa**

In strongly correlated electrons systems, many exotic phenomena such as high-$T_c$ superconductivities have been found. To clarify how the strongly electronic correlations induce such exotic phenomena, highly-accurate numerical methods for the low-energy effective models of strongly correlated electron systems such as Hubbard model play essential role. For the ground-state calculations (zero-temperature calculations), powerful numerical algorithms such as density matrix renormalization group method or tensor network algorithms already exist and they have been applied to broad range of the strongly correlated electrons systems. However, for the finite-temperature calculations, the efficient numerical method is absent and development of highly-accurate finite-temperature calculations remains a challenging problem.

In the textbook implementation of the finite-temperature calculation, it is necessary to take ensemble average over the excited states and it is practically formidable to carry out. Contrary to the standard implementation, recent development of the statistical physics shows that the calculation within small number of pure states instead of the full ensemble average is sufficient for accurate estimate of finite-temperature properties. Such pure states are called thermal pure quantum (TPQ) states and they are easily generated by performing the imaginary-time evolution of the wave function.

Based on the principle of the TPQ, we develop a new method to perform the calculations for the larger system

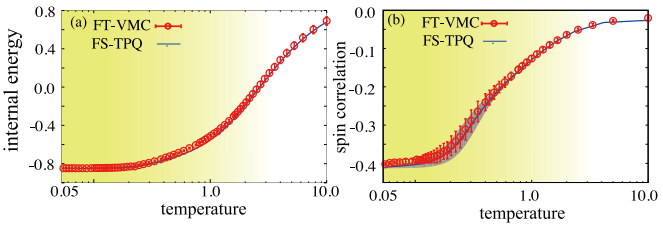


Fig. 1. (a) Temperature dependence of internal energy per site calculated from FT-VMC for 4×4 half-filled Hubbard model with $U/t$=4. The FT-VMC result is shown by red circles in comparison with essentially exact results obtained by full-space TPQ (FS-TPQ) method shown by blue curve. (b) Temperature dependence of nearest neighbor spin correlations calculated by FT-VMC (red circle) and FS-TPQ (blue curve) method. The shadow region in (a) and (b) represent the error bars in FS-TPQ method.

size where the exact imaginary-time evolution is impossible. A key fact is that accurate imaginary-time evolution of the wave functions is possible by using the stochastic reconfiguration method, which is used as the optimization method in the variational Monte Carlo (VMC) method. Thus, we call this numerical method finite-temperature VMC (FT-VMC) method. By comparing the exact results, as shown in Fig. 1, we have shown that temperature dependence of the physical properties such as internal energy and spin correlations is well reproduced by using the FT-VMC method. Moreover, we have shown that our method can be applicable to larger system size where the exact imaginary-time evolution is impossible. Our method opens a new way for the accurate calculations of the strongly correlated electron systems.

**Reference**
[1] K. Takai, K. Ido, T. Misawa, Y. Yamaji, and M. Imada, J. Phys. Soc. Jpn. **85**, 034601 (2016).

**Authors**
K. Takai[a], K. Ido[a], T. Misawa, Y. Yamaji[a], and M. Imada[a]
[a]University of Tokyo

# Capturing Transiently Charged States at the C60/TiO2(110) Interface by Time-Resolved Soft X-ray Photoelectron Spectroscopy

**K. Ozawa, S. Yamamoto, and I. Matsuda**

One of key technologies for realizing sustainable society is an efficient conversion of the sunlight into chemical and electrical energies. Titanium dioxide ($TiO_2$) exhibits a high photocatalytic activity for water splitting to produce a zero-emission fuel. $TiO_2$ is also used as a transparent electrode in photovoltaic cells [2]. One of the extensively studied $TiO_2$-based photovoltaic cells is a dye-sensitized organic cell, in which visible-light sensitive dye molecules or polymers are loaded onto the $TiO_2$ electrodes. The $TiO_2$ electrode collects photoexcited electrons from the light absorbing layer to facilitate electron-hole separation. In such a photovoltaic cell, a charge transfer across the interface is an important elemental step to define the performance of the cell. A molecule of $C_{60}$ is an important component of dye-sensitized photovoltaic cells, where the $C_{60}$ layer is used as an electron acceptor and as an electron transport layer. $C_{60}$ also serves to enhance photocatalytic activity of $TiO_2$ by promoting the separation of the photoexcited electron-hole pairs. In the present study, we apply time-resolved soft X-ray photoelectron spectroscopy (TRPES) to the $C_{60}/TiO_2$ (110) heterojunction in order to elucidate how the excited carriers behave at the junction. An experiment of TRPES utilizing the pump-probe method has been proven to be a powerful tool to simultaneously determine the electronic structure and the dynamics of the photoexcited carriers at semiconductor surfaces.

The TRPES measurements were carried out at SPring-8 BL07LSU [1]. For the pump light, a second harmonic of an amplified Ti:sapphire laser pulse was used. The pulse duration and a repetition rate were 35 fs and 1 kHz, respectively. The photon energy was set at 3.06 eV, which exceeds both the band gap of rutile $TiO_2$ (3.0 eV) and the energy difference between the highest occupied molecular orbital (HOMO) level and the lowest unoccupied molecular orbital (LUMO) level of $C_{60}$ (2.3 eV). For the probe light, synchrotron radiation (SR) lights with the energies of 253 eV and 600 eV were used to measure valence-band spectra and Ti 2p and C 1s core-level spectra, respectively. The SR lights were provided by a single bunch and a 11/29-filling bunch train of an H-mode operation. SR pulses from the single bunches were used for the pump/probe measurements. A width of the pulse was 50 ps and a time interval between the pulses was 4.79μs.

We examined the effect of UV laser irradiation on the electronic structure of the $C_{60}/TiO_2$(110) heterojunction[2]. An upper panel in Fig. 1 shows a Ti $2p_{3/2}$ spectrum measured without UV irradiation. A background subtracted peak is reproduced by a single Voigt function with a peak maximum at 458.2 eV. A Ti $2p_{3/2}$ spectrum in the lower panel is acquired at 1ns after laser pulse irradiation. The peak is also fitted by a Voigt function with a peak maximum at 458.3 eV. Regarding the C 1s core-level peak of $C_{60}$, a laser induced shift is 0.25 eV towards the higher binding energy (BE) side. The C 1s peak in the dark condition (without laser irradiation) is located at 284.4 eV. A small structure at 286.1 eV is due to C–O. The peak moves to 284.65 eV at 1 ns after irradiation. The BE shifts of both Ti $2p_{3/2}$ and C 1s peaks are transient because the peaks go back to the original positions

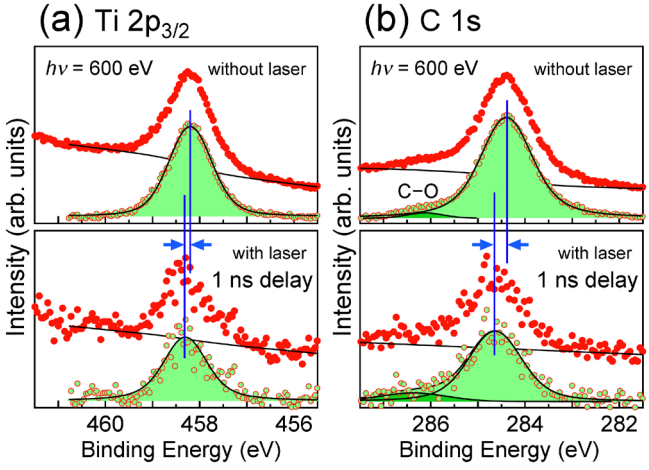


Fig. 1. (a) Ti $2p_{3/2}$ and (b) C 1s core-level spectra for $C_{60}/TiO_2$(110) with the $C_{60}$ thickness of 0.57 nm. Spectra in the upper panels were acquired without the pump laser, whereas those in the lower panels were measured at 1 ns after irradiation of the laser pulse. The photon energy of the pump laser was 3.06 eV, and a power density was 40μJ/cm2/pulse. The photon energy of the probe SR light was 600 eV, and the emitted photoelectrons were collected with repetition rates of 208 kHz for the upper spectra and 1 kHz for the lower spectra. In each panel, a raw spectrum and a background-subtracted spectrum are drawn by dots. Background curves, shown by solid lines, were a combination of a Shirley-type curve and a linear line. Solid lines with shaded areas are the result of least-square fitting using Voigt functions.

by the time the next probe pulse arrives after 4.79 μs. The energy shift does not due to the surface photovoltage (SPV) effect since direction of the energy shift is opposite to the expectation. Moreover, the power density of the irradiated pump laser in the present study was 40μJ/cm2/pulse, which was insufficient to induce the SPV effect on the $TiO_2$(110) surface [1].

Figure 1 clearly demonstrates that deposited $C_{60}$ on $TiO_2$(110) must be responsible for the UV-induced shift of the Ti $2p_{3/2}$ core level in the weak excitation condition. Aside from the $TiO_2$ substrate, the $C_{60}$ overlayer also absorbs the 3.06-eV pump laser. In the present excitation condition, the HOMO → LUMO+1 and HOMO-1 → LUMO transitions are possible so that the valence electrons should promote to the LUMO and LUMO+1 levels, and the holes are left in the HOMO and HOMO-1 levels. Since both the LUMO and LUMO+1 states energetically overlap to the conduction band of $TiO_2$, a resonant transfer of the excited electrons is possible from $C_{60}$ to $TiO_2$. Such an interface charge transfer competes with the electron-hole recombination process. It is speculated that a large fraction of the photoexcited electrons in the $C_{60}$ layer is possible to be transferred to $TiO_2$. The transferred electrons, then, undergo deexcitation to the bottom of the conduction band of $TiO_2$. As a result, $C_{60}$ is cationized after laser irradiation. The C 1s peak shift towards the higher BE side must, therefore, be caused by this charging effect. Regarding the $TiO_2$ side of the heterojunction, additional electrons are injected from the $C_{60}$ layer so that the carrier density is increased at the $TiO_2$ surface. The BE shift of the Ti $2p_{3/2}$ peak should, therefore, reflect the enlarged magnitude of downward band bending.

**References**

[1] M. Ogawa *et al.*, Rev. Sci. Instrum. **83**, 023109 (2012).
[2] K. Ozawa *et al.*, Organic Electronics **31**, 98 (2016).

**Authors**

K. Ozawa[a], S. Yamamoto, R. Yukawa, K. Akikubo, M. Emori[b], H. Sakama[b],and I. Matsuda
[a]Tokyo Institute of Technology
[b]Sophia University